2012 MRS FALL MEETING

Quantitative Defect Analysis on Solar Cells by Laser Beam Induced Current (LBIC) Measurements and 3D Network Simulations

Journal:	*2012 MRS Fall Meeting*
Manuscript ID:	Draft
Manuscript Type:	Symposium E
Date Submitted by the Author:	n/a

Complete List of Authors:	Nguyen, Minh; Robert Bosch GmbH, Corporate Research Schütt, Andreas; Christian-Albrechts-University, Institute for Materials Science Carstensen, Jürgen; Christian-Albrechts-University, Institute for Materials Science Föll, Helmut; Christian-Albrechts-University, Institute for Materials Science

Keywords:	photovoltaic, simulation, thin film

Quantitative Defect Analysis on Solar Cells by Laser Beam Induced Current (LBIC) Measurements and 3D Network Simulations

Minh Nguyen,[1,2] Andreas Schütt,[2] Jürgen Carstensen,[2] and Helmut Föll[2]
[1]Corporate Research, Robert Bosch GmbH, Stuttgart, Germany
[2]Institute for Materials Science, Christian-Albrechts-University, Kiel, Germany

ABSTRACT

Measurements with the CELLO (solar cell local characterization) technique in the LBIC (laser beam induced current) mode under dark conditions with various constant bias voltages are used to analyze the lateral distribution, and mean values, of photocurrent response maps.
Local solar cell defects such as local shunts were found to have a characteristic bias voltage dependence: At negative and small positive voltages a local shunt resistance gives less current response than the adjacent area. Upon applying higher positive voltages, a transition of the mean value to lower current response and an inversion of the local defect characteristics are found.
These results were modeled by a newly introduced three dimensional (3D) equivalent circuit model of a solar cell divided into subcells.
Measurements and simulations of solar cells with various local defects show our method to be a new powerful tool for the quantitative analysis of local solar cell defects.

INTRODUCTION

Thin film photovoltaic technologies, like CIGS, thin-film silicon or organic photovoltaics (OPV) offer the potential of low-cost production at relatively high efficiency levels [1].
Scaling up from lab cell sizes to mass production relevant sizes requires production and quality control on the whole area of the solar cell taking into account coating induced defects, edge shunting effects etc. Therefore, imaging methods like electro- and photoluminescence [2], thermography [3, 4] or light beam induced current (LBIC) [5, 6] and its further development CELLO [7] become more and more important. However, a quantitative analysis of local solar cell defects is still difficult as it usually requires a sophisticated calibration of the obtained images [8] or extensive numerical (device) simulations [9].
In the present work, the CELLO technique is used to unambiguously identify local defects as reduced shunt resistances and provides the possibility to quantify them.

EXPERIMENT

The CELLO technique is applied to microcrystalline thin film silicon (μc-Si) solar cells. The laser induced current responses at different constant bias voltages are measured at switched off global illumination. A scheme of the measurement setup is depicted in Fig. 1. The potentiostat unit together with the feedback control allow for very accurate current measurements while guaranteeing a constant bias voltage.

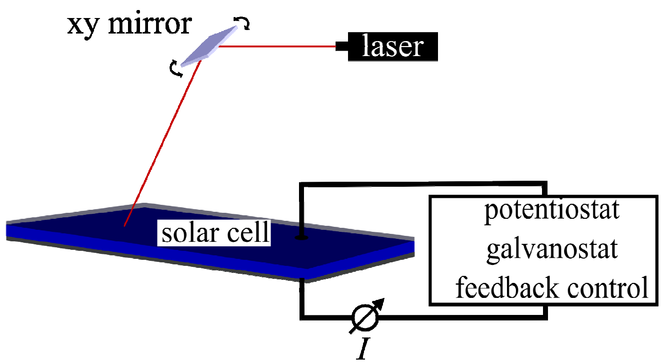

Fig. 1: Scheme of the CELLO measurement setup. A red laser of λ = 658 nm was used.

In Fig. 2 the measured current response of the µc-Si cell at different constant bias voltages is shown. Near the cell center a very prominent defect is marked by a pink circle. At negative and small positive bias voltages this defect gives less current response than the surrounding and therefore appears black. At higher bias voltages, around 0.7 V, the defect gives more current signal than the adjacent area and therefore changes its color from black to red. Additionally, a four-fold symmetry evolves, originating from the transparent conductive oxide (TCO) contact geometry at the four solar cell edges and the resulting voltage drop over the TCO. This effect was further investigated in [10] and is not part of this paper.

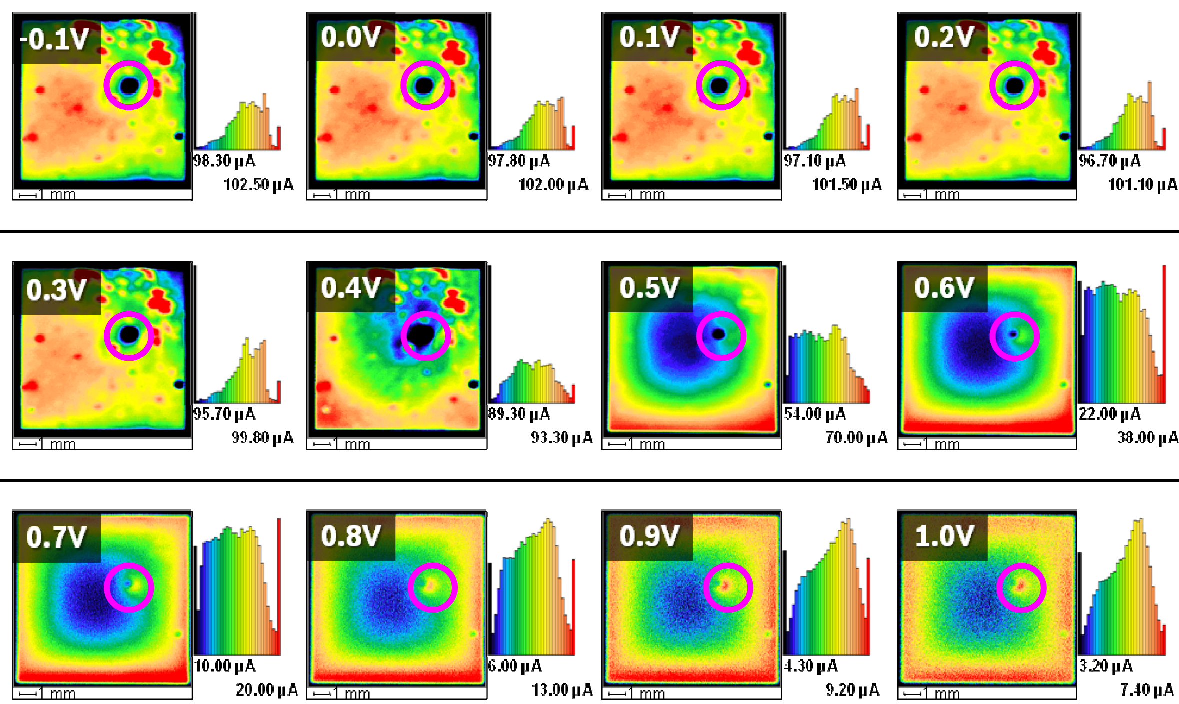

Fig. 2: Current response (dI) maps obtained by CELLO at different constant bias voltages. The pink circle marks the position of a local defect. Around 0.7 V the defect color changes from black to red. At voltages below 0.7 V the defect gives less signal than the adjacent area and reverses its behavior at higher bias voltages.

SIMULATION

For the simulations, a 3D equivalent circuit network is used and shown in Fig. 3. The squared solar cell is modeled with SPICE by a resistance network and by subcells connected in parallel, already described in [10]. The CELLO measurement is modeled by the following procedure: For all subcell positions (*i,j*) the difference of the total current *I with* local photocurrent at (*i,j*) and total current *without* local photocurrent is calculated:

$$dI_{ij}(V) = I\left(V, \left\{I_{kl}^{\text{laserON},ij}\right\}\right) - I\left(V, \left\{I_{kl}^{\text{laserOFF}}\right\}\right) \tag{1}$$

with

$$I_{kl}^{\text{laserON},ij} = I_{kl}^{\text{laserOFF}} + \delta_{ik}\delta_{jl}\Delta I_{ph} \tag{2}$$

and I_{kl}^{laserOFF} is the total current flowing through the subcell at position (*k,l*) without laser illumination.

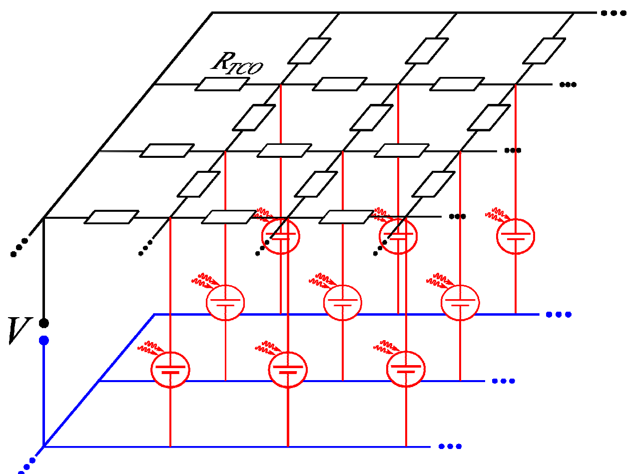

Fig. 3: Equivalent circuit model for the simulation: The TCO at the front contact is replaced by a resistance network built up of equal resistances R_{TCO}.

DISCUSSION

The network model (Fig. 3) is extended to implement local defects on the equivalent circuit model level. Therefore, the effect of parameter variations of the one- or two-diode-model in single subcells (shunt resistance R_p, series resistance R_s, diode backward current I_0 and the ideality factor *n*) can be analyzed on a spatially resolved scale. In general, such simulation can always be used to analyze measured data by varying the model parameter until all measured data are reproduced by the simulated data. Such kind of inversion is very time consuming. In what follows a simple way will be discussed how some kind of master curve extracted from the simulation can be used to directly analyze shunts quantitatively.

Simulations of a locally reduced shunt resistance near the cell center at different constant bias voltages show the same color-change at that certain position as observed experimentally, see Fig. 4. This color-change at positive voltages is unique for a reduced shunt resistance and cannot be modeled with defects related to R_s, I_0, or *n* (not shown here). Therefore, the defect in Fig. 3 has to be a locally reduced shunt resistance.

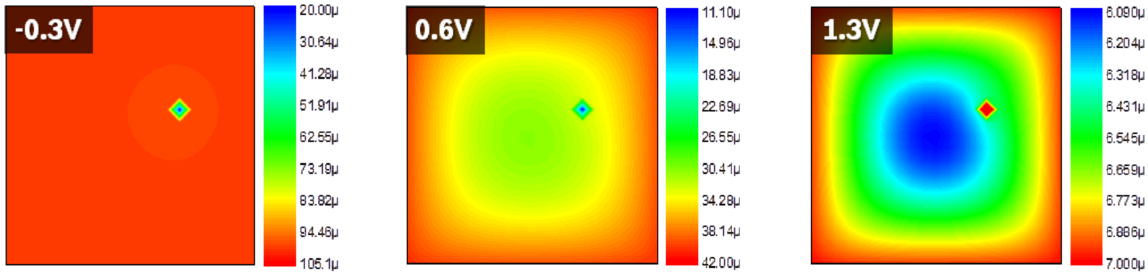

Fig. 4: Simulations of CELLO current response measurements at different constant bias voltages. The simulated defect undergoes the identical color-change as the one marked in Fig. 2, only observable for the failure mechanism of a locally reduced shunt resistance.

The voltage dependent current response can generally be described by the transfer function f [10], that is given by equation (3):

$$f \equiv \frac{dI}{dI_{ph}} = \frac{-1}{1 + \frac{R_s}{R_p} + \beta e R_s \sum_{i=1,2} \frac{I_{0i}}{n_i} \exp\left(\frac{\beta e (V - R_s I)}{n_i}\right)} \tag{3}$$

A typical curve shape of the transfer function for a regular solar cell and a shunted solar cell is shown in Fig. 5. In linear approximation, the CELLO signal dI is proportional to the absolute value of the transfer function:

$$dI = dI/dI_{ph} \cdot \Delta I_{ph}\,, \tag{4}$$

where ΔI_{ph} is the photocurrent induced by the laser. At negative and small positive voltages, the absolute value of f is larger for the unshunted cell (blue area). At voltages larger than a certain voltage, the transition voltage V_T, the shunted solar cell has a larger absolute value of f (red area). Therefore, a shunted subcell in a network of subcells connected in parallel with regular shunt resistances $R_{p,0}$ turns red at V_T. The simulations of the local electrical potential show that V_T is not a special voltage of sign reversal of the shunt behavior but is only determined by the intersection of two different transfer functions. Thus the transition voltage V_T can be used as an easy measurable number to quantify local shunts directly.

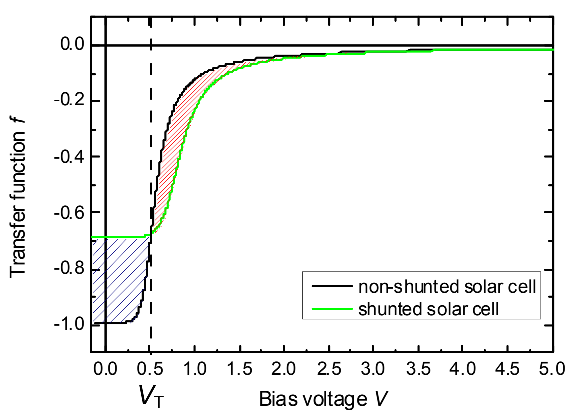

Fig. 5: Comparison of typical transfer functions of a non-shunted solar cell with a regular shunt resistance (black line) and a shunted solar cell with a reduced shunt resistance (green line). At the transition voltage V_T, both lines intersect.

The transition voltage V_T is numerically calculated by the intersection of two transfer functions of different shunt resistances:

$$f_{Rp,0}(V_T) = f_{x*Rp,0}(V_T)\ , \qquad (5)$$

where $R_{p,0}$ is the regular shunt resistance of a subcell and x the fraction of $R_{p,0}$.

In this work, 10000 intersections were calculated. As examples, four of them are depicted in Fig. 6. Clearly, the voltage of intersection V_T (marked by pink crosses) increases for lower shunt resistances. The curve of the transition voltages vs. shunt resistances is shown in Fig. 7. With this graph, valid for all solar cells with identical production conditions, the strength of one or multiple shunt resistances can be obtained quantitatively.

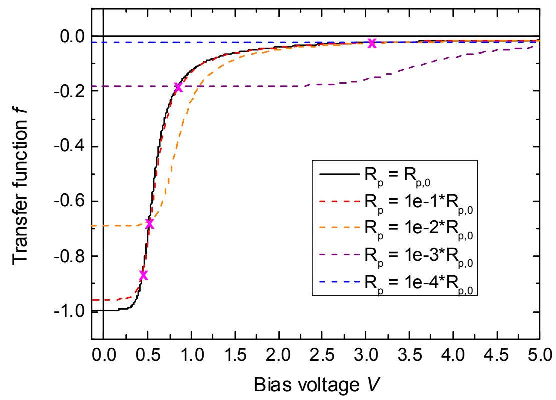

Fig. 6: Comparison of a transfer function with solar parameters obtained by a fit to an *IV* curve of an unshunted solar cell with $R_p = R_{p,0}$ (black solid line) and four examples of calculated transfer functions of different shunt resistance fractions $R_p = x*R_{p,0}$ (dashed lines). The pink crosses mark the corresponding transition voltages V_T.

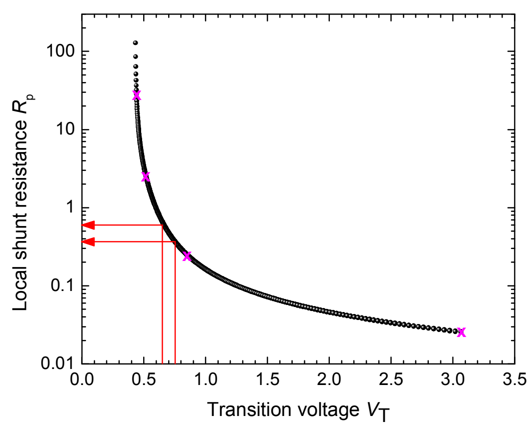

Fig. 7: 10000 calculated local shunt resistances $R_p = x*R_{p,0}$ with $R_{p,0} = 256.7\ \Omega m^2$ and their corresponding transition voltage. The red arrows mark the range of V_T for our measurement of around 0.7 V (0.65 V to 0.75 V), cf. Fig. 2, and the corresponding local shunt resistance R_p.

However, one needs to take care of the way of determining the parameters of the transfer function f by a fit to an *IV* curve of a solar cell. Ideally, f is determined from a defect-free solar cell which has been produced identically to the solar cell of which the shunt resistance should be quantified. This was provided by the μc-Si solar cells of the identical batch produced on the same glass substrate as our test cell.

For our test cell shown in Fig. 2 the transition voltage V_T is around 0.7 V. With the value of $R_{p,0} = 256.7\ \Omega m^2$ obtained from an *IV* curve fit of a one-diode model to an identically produced unshunted solar cell, the local reduced shunt resistance of our test cell can be estimated to a range of $0.37\ \Omega m^2$ to $0.66\ \Omega m^2$.

CONCLUSIONS

Locally reduced shunt resistances can be unambiguously identified in CELLO photo-current response maps by their bias voltage dependence. Simulations using an electrical 3D network and a two-diode model reveal that a defect showing a transition behavior in the strength of its photocurrent response for varying bias voltage – giving less/more signal than the adjacent area for lower/higher bias voltages – can only be modeled by a locally reduced shunt resistance R_p and not by other local mechanisms like R_s, I_0 or n losses. The relevant transition voltage V_T is determined by the intersection of the transfer functions of a non-shunted and a shunted cell.

Simulating transfer functions for various shunt resistances, a look-up table relating R_p and V_T can be generated, allowing to quantify an experimentally observed shunt from a measurement of its transition voltage. The transition voltage can be obtained from CELLO photocurrent response maps at different bias voltages. The parameters needed to set up the transfer function have to be obtained from a defect-free but identically produced solar cell by a one- or two-diode model based *IV* curve fit.

This method is a new powerful tool to quantitatively evaluate locally reduced shunts without the need for an extensive device simulation.

ACKNOWLEDGMENTS

The authors want to thank Dr. Jan-Martin Wagner for fruitful discussions and critical corrections of the manuscript.

REFERENCES

1. M.A. Green *et al.*, Prog. Photovolt.: Res. Appl. **20** (2012) 12-20.
2. R. Rösch *et al.*, Sol. Energy Mater. Sol. Cells **97** (2012) 176-180.
3. O. Breitenstein *et al.*, “Lock-in Thermography”, 2nd edition, Springer 2010.
4. H. Straube *et al.*, Sol. Energy Mater. Sol. Cells **95** (2011) 2768-2771.
5. P. Vorasayan *et al.*, Sol. Energy Mater. Sol. Cells **93** (2009) 917.
6. P. Vorasayan *et al.*, Sol. Energy Mater. Sol. Cells **95** (2011) 111-114.
7. J. Carstensen *et al.*, Sol. Energy Mater. Sol. Cells **76** (2003) 599-611.
8. M. Glatthaar *et al.*, Phys. Stat. Sol. RRL **4** (2010) 13-15.
9. S. Geißendörfer *et al.*, MRS Proc., 1321, mrss11-1321-a08-09
10. M. Nguyen *et al.*, Proc. 27th European Photovolt. Sol. Energy Conf., Frankfurt a. M., Germany (2012) 3DV.1.59